

# Characteristics of Plasma Current Start-Up by Transient Coaxial Helicity Injection on HIST

Takafumi HANAOK, Takahiro KAWAI, Yoshiharu UESAKA, Takaaki MATSUI, Yusuke KIKUCHI, Naoyuki FUKUMOTO and Masayoshi NAGATA

*Graduate School of Engineering, University of Hyogo, Hyogo 671-2280, Japan*

(Received 2 September 2015 / Accepted 14 November 2015)

Transient coaxial helicity injection (T-CHI) was successfully demonstrated in the Helicity Injected Spherical Torus (HIST) device for non-inductive plasma current start-up. The spherical torus (ST) requires no central solenoid coil. The characteristics of the T-CHI start-up discharges on the HIST were investigated in detail. The toroidal plasma current reached 60 - 80 kA, and the current density profile was significantly modified by variations in the bias poloidal coil flux. The Doppler ion temperature and electron temperatures reached 10 - 15 eV, and the electron density of  $1 \times 10^{20} \text{ m}^{-3}$ , depending on the bias flux. Internal magnetic field measurements using a two-dimensional magnetic probe array verified that closed flux surfaces formed after fast magnetic reconnection during the current rising phase. The amount of closed flux was quantitatively related to the bias flux. We also present the first experimental measurements of helicity balance during the T-CHI process. These results validate the capability of T-CHI for higher current generation in the ST.

© 2016 The Japan Society of Plasma Science and Nuclear Fusion Research

Keywords: spherical torus, coaxial helicity injection, non-inductive plasma current startup, coaxial plasma gun

DOI: 10.1585/pfr.11.1402001

## 1. Introduction

The spherical torus (ST) concept has been proposed for small, high-beta reactor designs. Omitting the Ohmic heating coil would simplify the design, and may be demanded by the small-diameter center post. Therefore, to realize the benefits of the ST concept, we require a non-inductive solenoid-less current start-up method. Coaxial helicity injection (CHI), previously developed in spheromak research, has been since applied to ST plasmas [1]. The applied CHI can be *driven* or *transient*. Driven CHI provides a steady-state current drive and relies on non-axisymmetric magnetic activity to drive the current through closed flux regions. The transient CHI (T-CHI) method requires only axisymmetric reconnection at the X point, and is believed to be adequate for generating a high-quality closed flux. A T-CHI method requiring no dynamo action is a promising candidate for non-inductive plasma start-up. In an NSTX application, the T-CHI yielded start-up ST plasma currents above 300 kA [2]. Furthermore, coupled discharge with inductive ramp-up has recently achieved plasma currents exceeding 1 MA [3].

The T-CHI method is based on the helicity conservation law of Taylor relaxation theory [4]. The helicity source is a magnetized coaxial plasma gun (MCPG), which injects plasma into the confinement region under the  $\mathbf{J} \times \mathbf{B}$  force. During the injection, the magnetic helicity  $K$ , defined as the linkage of the magnetic fluxes, is transferred from the MCPG to the confinement region. The injected magne-

tized plasma relaxes toward the ST equilibrium configuration with minimum energy. The helicity balance equation in the total system is given by

$$\frac{dK}{dt} = -K/\tau_K + 2V_{\text{gun}}\Psi_{\text{bias}}, \quad (1)$$

where  $\tau_K$  is the resistive dissipation rate of  $K$ ,  $V_{\text{gun}}$  is the voltage between the inner and outer electrodes, and  $\Psi_{\text{bias}}$  is the bias vacuum poloidal flux. Provided that the helicity injection rate ( $2V_{\text{gun}}\Psi_{\text{bias}}$ ) is larger than the dissipation rate,  $K$  increases as the plasma current dissipates, i.e., the poloidal flux is amplified during the current start-up.

T-CHI using the MCPG has recently been applied on the Helicity Injected Spherical Torus (HIST) [5]. The aim was to examine the performance of T-CHI as a non-inductive start-up method and to study the characteristics of the start-up plasma. Although the usefulness of the T-CHI method has already proven useful on NSTX, the physics of the flux closure and reconnection during T-CHI remain poorly understood. Internal magnetic field probe measurements in a smaller machine would confirm the generation of a closed flux. In this paper, we will show characterize the T-CHI start-up plasmas by examining the flux amplification, internal magnetic field structure, current density profiles, ion and electron temperatures, and density, which depends on the bias flux strength. The helicity balance of the ST plasmas produced by T-CHI and the helicity injection threshold are experimentally verified in this paper.

author's e-mail: eu13s003@steng.u-hyogo.ac.jp

## 2. Experimental Setup

### 2.1 HIST device

The major and minor radii of the designed HIST device are  $R = 0.3$  m and  $a = 0.24$  m, respectively. The aspect ratio  $A$  is 1.25 (Fig. 1). The toroidal field coil current  $I_{TF} = 135$  kA produces a vacuum toroidal field  $B_{t,v} = 0.09$  T at the magnetic axis. The HIST device is detailed in Ref. [5]. The T-CHI capacitor bank for discharges across the MCPG electrodes has a maximum charging voltage of 6 kV, a capacitance of 2.9 mF, and a stored energy of 52 kJ. For T-CHI, the injection current generated by the capacitor bank must exceed the bubble burst current, and the  $\mathbf{J} \times \mathbf{B}$  force must overcome the bias field tension. The bubble burst current requirement, i.e., the helicity injection threshold, is given by

$$I_{inj} = \frac{2\Psi_{bias}^2}{\mu_0^2 d^2 I_{TF}}, \quad (2)$$

where  $\Psi_{bias}$  is the bias flux at the MCPG,  $d$  is the bias flux footprint width, the  $I_{TF}$  is the total current in the toroidal field coil [1]. A successful T-CHI current drive also requires that the force-free parameter  $\lambda$  of the MCPG ( $\lambda_{gun} = \mu_0 I_{gun} / \Psi_{bias}$ ) exceeds that of the ST plasma ( $\lambda_{ST} = \mu_0 I_t / \Psi_t$ ) [1]. This condition allows helicity transport from the higher to the lower  $\lambda$  region. The HIST device is designed to satisfy this condition.

### 2.2 Diagnostics

A Rogowski coil and a high voltage differential probe are installed on the MCPG to measure the gun current  $I_{gun}$  and the gun voltage  $V_{gun}$ . The toroidal plasma current  $I_t$  is measured by a 16-channel surface poloidal pick-up probe (Fig. 1). The toroidal current density and toroidal flux profiles at the mid-plane of the flux conserver (FC) are measured by an 8-channel  $\lambda$ -probe incorporating small-size Rogowski and flux loops.

To measure the time evolution of the poloidal flux  $\Psi_p$

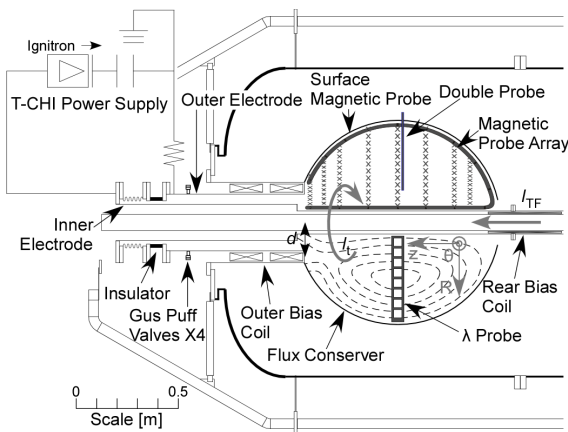


Fig. 1 Poloidal cross-section of the HIST device and 2D magnetic probe array.

contours, we inserted two-dimensional magnetic probe array (comprising  $85 \times B_z$  and  $85 \times B_t$  pick-up coils with  $\Delta R = 0.02$  m or  $0.05$  m and  $\Delta Z = 0.148$  m or  $0.074$  m) on the  $R$ - $Z$  poloidal plane, as shown in Fig. 1. Here,  $B_z$  and  $B_t$  are the axial components of the poloidal and toroidal fields, respectively. To obtain contours of the poloidal flux, we calculate  $\Psi_p(R) = 2\pi \int_0^R R B_z dR$ , assuming axisymmetric magnetic configurations. The flux contour plot yields the total (maximum) poloidal flux  $\Psi_{p,max}$ .

The electron temperature and density are measured by a double electrostatic probe. The probe current is measured by applying a triangular sweep voltage of up to 32 V of a triangle waveform with a frequency at 25 kHz or 100 kHz.

To measure the radial profile of the Doppler ion temperature  $T_{i,D}$  in the plasma, we developed a multi-point ion Doppler spectroscopic (M-IDS) system based on the single-point IDS system [6]. The M-IDS system uses a 1-m spectrometer (Ritsu Ouyou Kougaku Co., Ltd., MC-100N), including an 8-channel optical fiber with fiber core diameter of 0.4 mm (Mitsubishi Cable Industries, Ltd., STU400E-S). The detector is a high-speed camera (Photron Ltd., FASTCAM-SA4/SA5). The measurement chords are in the toroidal cross section at the mid-plane and their radii vary from 0.09 m to 0.39 m, as shown in Fig. 2. Each chord is separated by 0.05 m. When measured by a single-point IDS system with a 16-channel multi-anode photomultiplier tube (M-PMT) detector, the data from each chord during shot-by-shot discharge provide a spatial profile of  $T_{i,D}$ . The Doppler ion temperature is calculated by the full width at half maximum (FWHM) of the line broadening signal, where  $\lambda_{FWHM}$  is given by Eq. (3):

$$T_{i,D} = 1.67 \times 10^8 A \frac{\Delta\lambda_{FWHM}^2}{\lambda_0^2}, \quad (3)$$

where  $\lambda_0$  is the wavelength of the emitted line and  $A$  is mass number of the ions. The carbon impurity spectral line (CIII: 464.74 nm) was measured in this experiment.

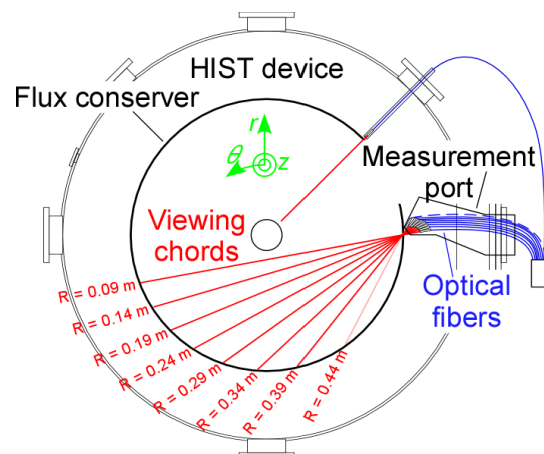


Fig. 2 Multi-channel ion Doppler spectroscopic (M-IDS) system. The M-IDS system is set on the mid-plane.

### 3. Experimental Results

#### 3.1 Typical start-up discharges by the T-CHI method

Figure 3 shows a typical shot of T-CHI current start-up on the HIST. In this shot, the MCPG receives an initial poloidal bias flux  $\Psi_{\text{bias}}$  of 1.75 mWb. The peak gun current  $I_{\text{gun}}$  of 75 kA is driven by the capacitor bank with a charging gun voltage  $E_{\text{gun}}$  of 5 kV. The  $I_{\text{inj}}$  is much larger than the critical current of 0.8 kA ( $d = 0.19$  m,  $\Psi_{\text{bias}} = 1.75$  mWb,  $I_{\text{TF}} = 135$  kA), which is calculated from the bubble-burest current requirement given by Eq. (2).

In Fig. 3, the toroidal current  $I_t$  increases up to 80 kA at  $t = 0.23$  ms. Figure 3(c) shows the rate of external helicity creation by the MCPG, given as  $dK_{\text{inj}}/dt = 2V_{\text{gun}}\Psi_{\text{bias}}$ . After the break-down of the puffing gas ( $\text{H}_2$ ) at  $t = 0.05$  ms,  $dK_{\text{inj}}/dt$  gradually increases to  $1.7$  Wb<sup>2</sup>/s. The total poloidal flux  $\Psi_p$  rapidly increases from its vacuum flux level of  $\Psi_{\text{bias}}$  (indicated by the dotted line in Fig. 3(d)) to  $\sim 3.8$  mWb at  $t = 0.12$  ms. This peak  $\Psi_p$  is maintained

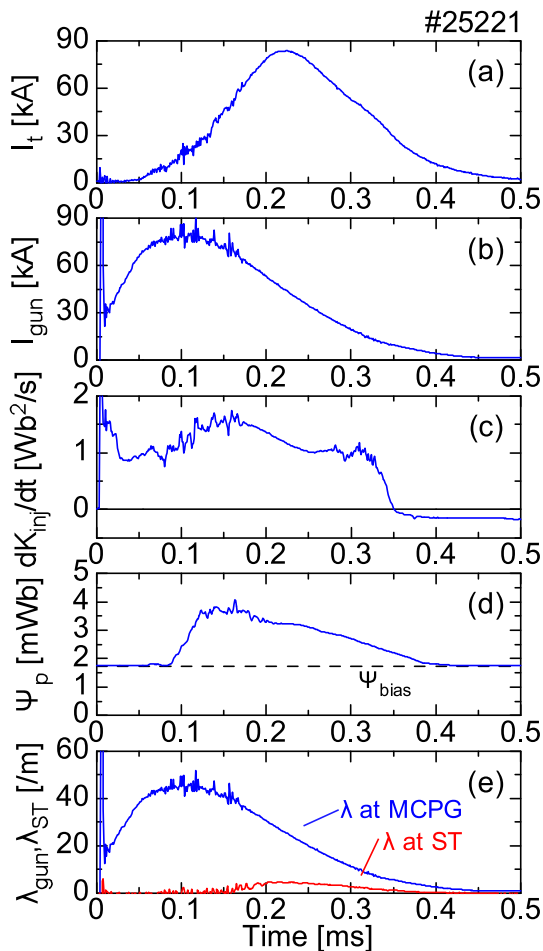


Fig. 3 Time evolution of (a) toroidal plasma current  $I_t$ , (b) gun current  $I_{\text{gun}}$ , (c) helicity injection rate, (d) poloidal flux  $\Psi_p$  and (e) pinch parameter of  $\lambda$  defined at the MCPG and FC for typical T-CHI discharges with  $E_{\text{gun}} = 5$  kV,  $\Psi_{\text{bias}} = 1.75$  mWb and  $I_{\text{TF}} = 135$  kA.

for a while, and then begins to decay from  $t = 0.25$  ms, along with  $I_t$ . At this time,  $I_{\text{gun}}$  falls below 30 kA and  $V_{\text{gun}}$  decreases to 0.3 kV, too low to inject helicity into the FC plasma. Based on these characteristics, we divide the plasma start-up process into three phases: an injection phase, in which the flux amplifies ( $0.05$  ms  $< t < 0.12$  ms); a sustainment phase ( $0.12$  ms  $< t < 0.3$  ms); and a decay phase ( $t < 0.3$  ms).

In the radial direction, the local  $\lambda_{\text{ST}} = \mu_0 I_t / \Psi_t$  is minimized at  $R = 0.19$  m, as shown in Fig. 3(e). Comparing this value with  $\lambda_{\text{gun}} = \mu_0 I_{\text{gun}} / \Psi_{\text{bias}}$  of the MCPG, we confirm that the condition  $\lambda_{\text{gun}} > \lambda_{\text{ST}}$  is satisfied.

#### 3.2 Time evolution of poloidal flux contours

Figure 4 shows the time evolution of the poloidal flux  $\Psi_p$  contours during the start-up phase. Figure 4(a) presents the bias flux  $\Psi_{\text{bias}}$  revealed by the poloidal flux contours at  $t = 0$  ms. Between 0.05 and 0.08 ms, the bias poloidal field lines are stretched by the plasma ejected from the MCPG. At that time, magnetic reconnection occurs around the entrance region of the FC, forming the plasmoid (closed flux) and X-point. The plasma expands and reaches the end of the FC (opposite side to the MCPG) at  $t = \sim 0.1$  ms. A new plasmoid, separate from the initial plasmoid, is then formed, i.e., double plasmoids are established in the FC. This T-CHI amplification process may be consistent with the plasmoid instability observed in a magnetohydrodynamic simulation [7]. Note that the flux contour at  $t = 0.25$  ms (during the decay phase) exhibits a magnetic configuration with a single closed flux region due to relaxation. The closed poloidal flux at this time ( $\sim 1$  mWb) was calculated from the flux contours.

#### 3.3 Time evolution of temperature and density profiles in T-CHI discharge

Figure 5 compares the plasma characteristics between high and low bias fluxes ( $\Psi_{\text{bias}} = 2.13$  mWb and 1.61 mWb, respectively). Under the low bias flux,  $I_t$  rises faster and reaches a higher peak than that under high flux bias. The time at which  $I_t$  peaks is also delayed under the higher bias flux. Two findings emerged from this experiment. First, the radial profile of the toroidal current density  $J_t(R)$  depends on the bias flux. In the low bias case (Fig. 5(b)), the current density  $J_t$  concentrates in the open central column (OFC) near the central conductor ( $0.1$  m  $< R < 0.15$  m), whereas in the high bias case (Fig. 5(c)), it remains relatively low and distributes at the interface between the closed flux and the OFC regions ( $0.15$  m  $< R < 0.2$  m). In both cases, the inner edge current diffuses toward the magnetic axis ( $R = 0.3$  m) after  $t = 0.35$  ms in the decay phase, forming peaked current profiles.

The other finding is the kink instability in  $J_t(R)$  under the low bias flux. The kink instability, occurring at  $t = 0.14$  ms, is accompanied by the distortion in the high-

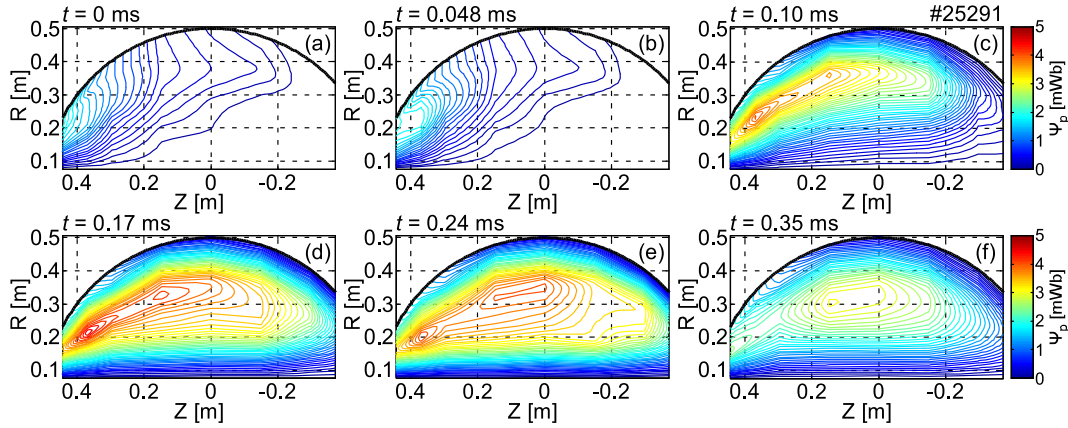


Fig. 4 Time evolution of poloidal flux contours in the FC, calculated for a typical T-CHI discharge with  $E_{\text{gun}} = 5$  kV,  $\Psi_{\text{bias}} = 2.13$  mWb (shown in (a)), and  $I_{\text{TF}} = 135$  kA.

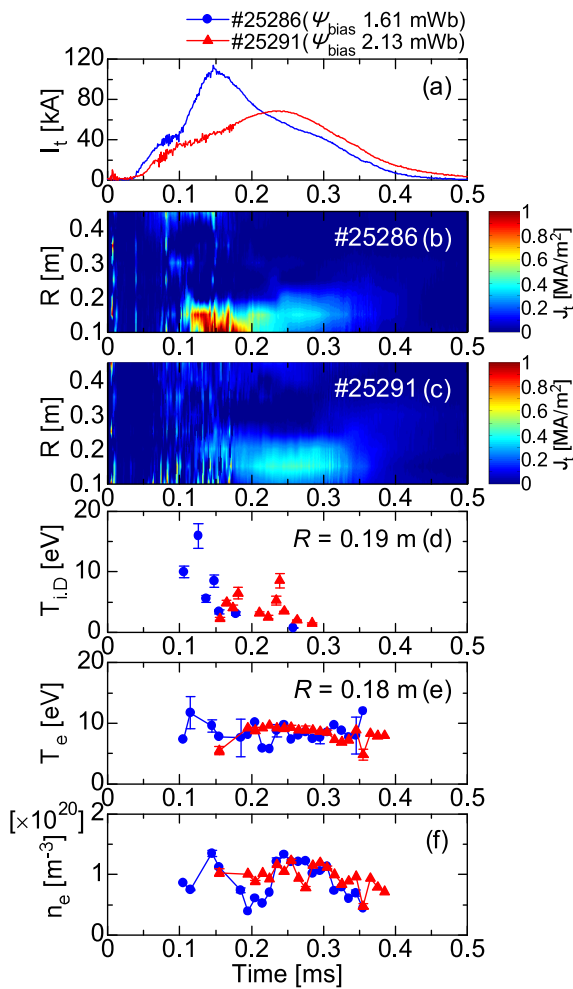


Fig. 5 Time evolution of (a) toroidal plasma current, (b) and (c) toroidal current density profile  $J_t(R)$ , (d) ion Doppler temperature  $T_{i,D}$ , (e) electron temperature  $T_e$  and (f) electron density  $n_e$ . These plots compare typical T-CHI discharge under a low bias flux ( $\Psi_{\text{bias}} = 1.61$  mWb) and a high bias flux ( $\Psi_{\text{bias}} = 2.13$  mWb).

intensity region of  $J_t(R)$  (see Fig. 5 (b)). As shown in the flux contours, the closed flux disappears at this time because the OFC region becomes helically deformed and violates the axisymmetric assumption. However, the distorted magnetic configuration relaxes back to an axisymmetric state during the decay phase.

As shown in Figs. 5 (d) and (e), the ion Doppler temperature  $T_{i,D}$  at the time of peak  $I_t$  is higher under the low flux bias (blue circles) than that under high bias (red circle), whereas the electron temperatures  $T_e$  are comparable. In both cases, the electron density  $n_e$  measured at  $R = 0.18$  m is approximately  $1 \times 10^{20} \text{ m}^{-3}$  (Fig. 5 (f)). However, note that in the low bias case, the density rapidly decreases at  $t = 0.14$  ms due to the instability and recovers to its original level at  $t = 0.25$  ms.

Figure 6 plots the radial profiles of  $T_{i,D}$  and  $T_e$  under the low bias flux, averaged in 0.04 ms. The  $T_{i,D}$  profile was measured by the IDS system. The  $T_{i,D}$  peaks in the 10-20 eV range in the OFC region during the injection and amplification phases ( $t = 0.06$ -0.14 ms). The relatively high  $T_{i,D}$  at  $R < 0.15$  m is likely attributable to the self-pinch effect of the large injection current flowing in the OFC (see Fig. 5 (b)). Thereafter,  $T_{i,D}$  decreases as the injection current decays, resulting in flat  $T_{i,D}$ . The low  $T_e$  in the 5-15 eV is attributed to the insertion of many magnetic probes. Between 0.18 to 0.22 ms, the  $T_{i,D}$  profile becomes slightly lower than the  $T_e$  profile.

### 3.4 Performances of T-CHI plasmas under changing bias flux

As the bias flux increases, the toroidal current should also increase because the helicity injection rate increases (by Eq. (1)). However, above the critical bias flux, the plasma cannot eject from the MCPG region. In other words, the bias field lines do not expand from the gun muzzle.

We studied the characteristics of the T-CHI generated

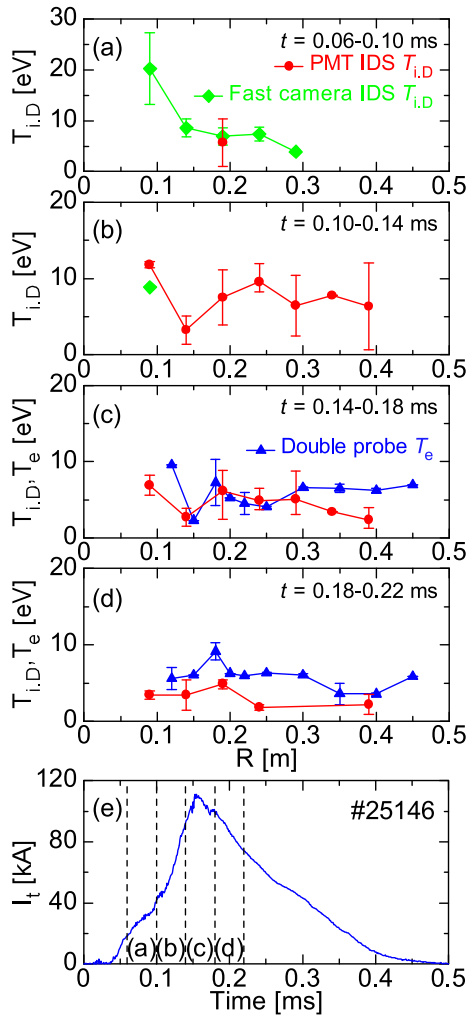


Fig. 6 Radial profiles of the ion Doppler temperature  $T_{i,D}$  (a)-(d) and electron temperature  $T_e$  (c) and (d) obtained from T-CHI discharges (e) under the low bias flux ( $\Psi_{\text{bias}} = 1.61$  mWb).

plasma by varying the strength of the bias flux. Figure 7 plots the maximum  $I_t$ , and  $\Psi_p$ , the closed poloidal flux  $\Psi_{p,\text{close}}$ , and the maximum ion and electron temperatures ( $T_{i,D}$  and  $T_e$  respectively), as functions of  $\Psi_{\text{bias}}$ . In the low flux bias regime ( $1.6 \text{ mWb} < \Psi_{\text{bias}} < 1.8 \text{ mWb}$ ),  $I_t$  peaks in the range 100-130 kA. Under high  $\Psi_{\text{bias}}$  ( $1.9 \text{ mWb} < \Psi_{\text{bias}} < 2.1 \text{ mWb}$ ), the peak  $I_t$  decreases to 60 kA. The critical  $\Psi_{\text{bias}}$  that affects the induced  $I_t$  appears to lie between 1.8 and 1.9 mWb. Unlike  $I_t$ ,  $\Psi_p$  increases with  $\Psi_{\text{bias}}$ . The closed poloidal flux  $\Psi_{p,\text{close}}$  was estimated as 1 mWb from the poloidal flux contours.  $\Psi_{p,\text{close}}$  probably depends on the bias flux strength. Figure 7 (b) plots the flux amplification ratio, defined by  $\Psi_p/\Psi_{\text{bias}}$ , as a function of bias flux. This ratio, computed as  $\Psi_p/\Psi_{\text{bias}} \sim 2.2$ , weakly depends on the bias flux, whereas  $\Psi_{p,\text{close}}$  is independent of  $\Psi_{\text{bias}}$ . Thus, as the bias flux increases, the ratio of the closed flux to the total flux slightly decreases from 30% to 25%, while  $T_{i,D}$  decreases from 15 eV to 8 eV. On the other hand,  $T_e$  is insensitive to  $\Psi_{\text{bias}}$ .

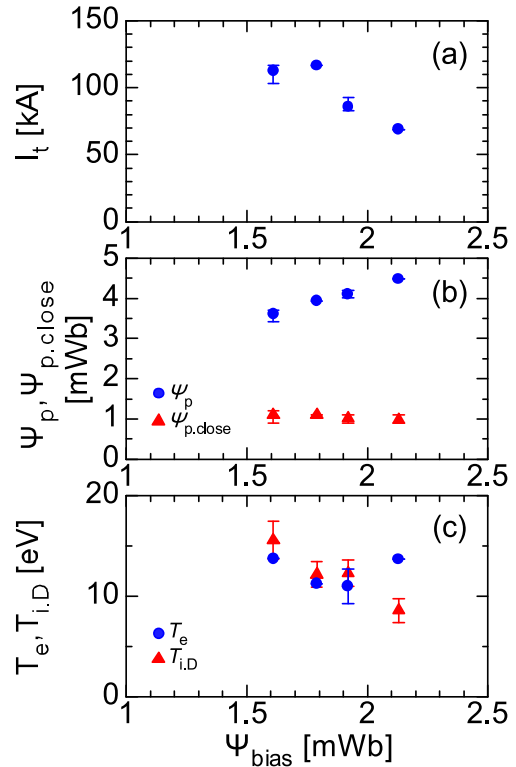


Fig. 7 Toroidal current  $I_t$  (a), total poloidal flux  $\Psi_p$  and closed poloidal flux  $\Psi_{p,\text{close}}$  (b), and ion and electron temperatures ( $T_{i,D}$  and  $T_e$  respectively) (c) as functions of the bias flux  $\Psi_{\text{bias}}$ .

## 4. Discussion

Having experimentally verified the helicity balance (Eq. (1)), we can predict the time dependence of the ST magnetic fields. The helicity balance between the MCPG (source) and ST plasma in the FC is determined by measuring the helicity created by the MCPG, the helicity content of the ST equilibrium plasma, and the resistive loss of the helicity. The general solution to Eq. (1) is given by [8]

$$K(t) = \exp(-t/\tau_K) \int_0^t 2V_{\text{gun}} \Psi_{\text{bias}} \exp(t'/\tau_K) dt', \quad (4)$$

where  $\tau_K$  is assumed constant. If the gun voltage  $V_{\text{gun}}$  and bias flux  $\Psi_{\text{bias}}$  are known, we can determine the source helicity injection rate  $dK_{\text{inj}}/dt$  and the helicity dissipation rate  $\tau_K$ , and thus, predict the time-dependent ST helicity content  $K(t)$ . Comparing predicted and measured helicity, we can determine the helicity conservation [4]. The measured helicity injection rate is plotted in Fig. 3 (c). By definition,  $\tau_K$  is related to the usual resistive decay rate  $\tau_W$  of the magnetic energy  $W = B^2/2\mu_0$ . According to the Taylor model, the plasma relaxes toward the force-free equilibrium  $\nabla \times \mathbf{B} = \lambda \mathbf{B}$  through a turbulent process (where  $\lambda = W/K$ ), and then remains in the minimum energy state with  $\lambda = \text{constant}$  during the decay phase. In this model,  $K$  decays only by resistivity and does not dissipate by relaxation during the helicity injection phase. The  $K$  resistive

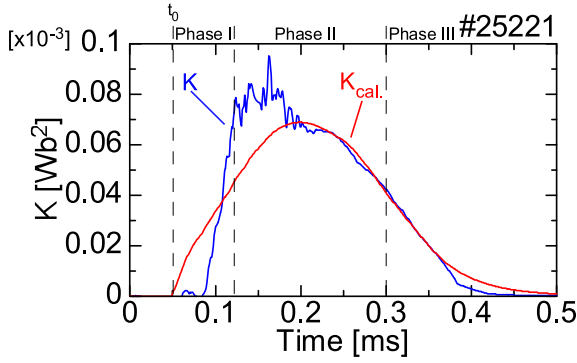


Fig. 8 Comparison of the measured (blue) and predicted (red) helicity contents  $K$  and  $K_{\text{cal}}$ , respectively. The latter is calculated by Eq. (4).

decay rate  $\tau_K$  is equal to  $\tau_W$  to half of the magnetic field decay rate  $\tau_B = B/(dB/dt)$ , and so we write  $\tau_K = \tau_W = \tau_B/2$  [8]. The helicity content  $K$  of the ST plasma is approximately computed as  $K \sim \Psi_p \Psi_t - \Psi_{\text{bias}} \Psi_{t,v}$ , where the subtracted term is contributed by the vacuum components of  $\Psi_{\text{bias}}$  and  $\Psi_{t,v}$  [9]. Here,  $\Psi_{t,v}$  is the vacuum toroidal flux.

We now discuss the helicity balance and the helicity injection threshold during the current rise (phase I), sustainment (phase II), and decay (phase III). The helicity injection threshold is relevant only in phase I. Figure 8 compares the predicted and measured helicities of the ST. The time dependences of the measured and predicted  $K_{\text{cal}}$  with  $\tau_K = 0.05$  ms agree during the decaying phase III. However, early in time, the predicted value does not appear to fit the time dependence of the rise during the phase I and of former half of the phase II. In particular, the time of initial  $K$  increase is delayed in the measurement, and rise is faster than predicted. This difference relates to the helicity injection threshold for the gun operation, calculated by Eq. (2). The helicity injection threshold exists because the  $\mathbf{J} \times \mathbf{B}$  force must overcome the magnetic tension of the bias field. Prior to exceeding this threshold, the generated helicity is expended in discharge generation in the MCPG region, and does not contribute to the helicity injected into the FC to form the ST. Once the injection current has exceeded the threshold, the helicity in the MCPG is rapidly transported to the FC region through the bubble burst event. During this discharge, the plasma generated in the MCPG begins expanding in the FC at  $t \sim 0.08$  ms. To exclude the initial gun voltage spike before  $t \sim 0.05$  ms, caused by the breakdown of the puffing gas, the integration in Eq. (4) is performed from  $t_0 = 0.05$  ms. If Eq. (4) is integrated over a much shorter time than  $\tau_K$ , the resistive dissipation is negligible. After the injection, the ST equilibrates and the resistive dissipation of  $K$  becomes effective, but is balanced by the increase  $K$  in phase II. Namely, the current amplification is balanced by the current dissipation due to resistivity. During phase III, the MCPG becomes isolated from the FC region after  $t = 0.3$  ms and the heli-

city decays resistively with  $\tau_K = 0.05$  ms.

Resistive decay is related to the conductivity electron temperature  $T_{e,\text{con}}$  by Spitzer resistivity  $\eta_{\text{spitzer}}$  scaling. The toroidal electric field  $E_t$  induced at the magnetic axis ( $R = R_{\text{axis}}$ ) during the decay phase was estimated from  $E_t = V_t/2\pi R_{\text{axis}}$  as 5.3 V/m, where the toroidal loop voltage  $V_t = \Psi_{p,\text{close}}/\tau_B$  was approximately 10 V ( $\sim 1$  mWb/0.1 ms) and  $R_{\text{axis}}$  was 0.3 m. From  $E_t = \eta_{\text{spitzer}} \Delta J_t$  (where  $\Delta J_t$  is the decrement in the current density  $J_t$  at  $R = R_{\text{axis}}$ , estimated as  $\sim 0.1$  MA/m<sup>2</sup>),  $\eta_{\text{spitzer}}$  was obtained as  $5.2 \times 10^{-5} Z_{\text{eff}} \ln \Lambda T_{e,\text{con}}^{-3/2}$ , where  $Z_{\text{eff}}$  is the effective  $Z$  and  $\ln \Lambda$  is the Coulomb logarithm (typically  $\sim 10$ ). Assuming  $Z_{\text{eff}} = 1-3$  and given  $\eta_{\text{spitzer}} \sim 5.3 \times 10^{-5} \Omega\text{m}$ , the conductivity temperature  $T_{e,\text{con}}$  was estimated as 5–10 eV. This value is consistent with the measured  $T_e$ . Hence, we consider that  $\tau_K = \tau_B/2 = 0.05$  ms is a reasonable resistive decay rate for  $K_{\text{cal}}$ . The estimated  $\tau_B$  is the resistive component of the  $L/R$  time of the ring current, where  $L$  and  $R$  are its inductance and resistance, respectively. These values were calculated as  $L = V_t/(S \Delta J_t/\tau_B)$  and  $R = 2\pi R_{\text{axis}} \eta_{\text{spitzer}}/S$ , where  $S$  is the cross-section of the current ring. Consequently,  $\tau_{L/R} = L/R = \tau_B V_t/(2\pi R_{\text{axis}} E_t) = \tau_B$ .

## 5. Conclusions

We investigated the characteristics of T-CHI start-up discharges on HIST. The results are summarized below:

1) As demonstrated in the internal magnetic field measurements, a closed flux can form after the magnetic reconnection. The closed flux  $\Psi_{p,\text{close}}$  was measured as 1 mWb, composed 25%–30% of the total flux. Although the poloidal flux increased with the bias flux, the flux amplification ratio ( $\Psi_p/\Psi_{\text{bias}} \sim 2.2$ ) was independent of the bias flux.

2) The current density profile depends on the bias flux. Under low bias flux, the generated current peaked at over 100 kA. The kink instability observed in the central open flux region may have been caused by the large injection current along the open field lines. The equilibrium configuration was stabilized in the high bias flux regime, but the plasma current decreased to 60–80 kA and the ion temperature also decreased.

3) Under low bias flux, the ion temperature  $T_{i,D}$  in the OFC region was relatively high during the early discharge. This finding may explain the pinch effect, by which the injection current compresses the OFC. The electron temperature  $T_e$  exhibited a flat profile that was independent of the bias flux strength.

4) We experimentally verified the helicity balance based on the conservation of magnetic helicity. From this important result, we can determine the magnitude and time dependence of the magnetic fields created by T-CHI. Here, we examined the balance between the MCPG helicity source and the ST in the FC by comparing the measured helicity  $K$  with that determined by Eq. (4) throughout the T-CHI start-up process. The resistive diffusion time  $\tau_K$

was estimated from the classical resistivity  $\eta_{\text{spitzer}}$  and the measured helicity injection rate  $dK_{\text{inj}}/dt$ . From the helicity balance model, we can predict the evolution of the poloidal flux.

## Acknowledgments

The authors are grateful to R. Raman for many valuable discussions and suggestions. The authors also thank with A.C. Hossack, B.S. Victor, B.A. Nelson, T.R. Jarboe and HIT-SI team of University of Washington for the collaboration with development of the M-IDS system. This work was partially supported by Japan/U.S. Cooperation

in Fusion Research and Development.

- [1] T.R. Jarboe, *Fusion Technol.* **15**, 7 (1989).
- [2] R. Raman *et al.*, *Nucl. Fusion* **47**, 792 (2007).
- [3] R. Raman *et al.*, *Phys. Rev. Lett.* **104**, 095003 (2010).
- [4] J.B. Taylor, *Rev. Mod. Phys.* **58**, 741 (1986).
- [5] M. Nagata *et al.*, *Phys. Plasmas* **10**, 2932 (2003).
- [6] P. Gu *et al.*, *Rev. Sci. Instrum.* **75**, 1337 (2004).
- [7] F. Ebrahimi and R. Raman, *Phys. Rev. Lett.* **114**, 205003 (2015).
- [8] C.W. Barnes *et al.*, *Phys. Fluids* **29**, 3415 (1986).
- [9] T.H. Jensen and M.S. Chu, *Phys. Fluids* **27**, 2881 (1984).